ELSEVIER

Brain Research 750 (1997) 25–40

BRAIN RESEARCH

Research report

NMDA-R1 subunit of the cerebral cortex co-localizes with neuronal nitric oxide synthase at pre- and postsynaptic sites and in spines

Chiye Aoki [a,b,*], Julianne Rhee [a], Mona Lubin [a], Ted M. Dawson [c]

[a] *Center for Neural Science, New York University, New York, NY 10003, USA*
[b] *Biology Department, New York University, New York, NY 10003, USA*
[c] *Departments of Neurology and Neuroscience, The Johns Hopkins University School of Medicine, Baltimore, MD 21287, USA*

Accepted 17 September 1996

Abstract

The majority of nitric oxide's (NO) physiologic and pathologic actions in the brain has been linked to NMDA receptor activation. In order to determine how the NO-synthesizing enzyme within brain, neuronal NO synthase (nNOS), and NMDA receptors are functionally linked, previous studies have used in situ hybridization techniques in combination with light microscopic immunocytochemistry to show that the two are expressed within single neurons. However, this light microscopic finding does not guarantee that NMDA receptors are distributed sufficiently close to nNOS within single neurons to allow direct interaction of the two. Thus, in this study, dual immuno-electron microscopy was performed to determine whether nNOS and NMDA receptors co-exist within fine neuronal processes. We show that nNOS and the obligatory subunit of functional NMDA receptors, i.e. the NMDA-R1, co-exist within dendritic shafts, spines and terminals of the adult rat visual cortex. Axon terminals form asymmetric synaptic junctions with the dually labeled dendrites, suggesting that the presynaptic terminals release glutamate. Axons and dendrites expressing one without the other also are detected. These results indicate that it is possible for the generation of NO to be temporally coordinated with glutamatergic synaptic transmission at axo-dendritic and axo-axonic junctions and that NO may be generated independently of glutamatergic synaptic transmission. Together, our observations point to a greater complexity than previously recognized for glutamatergic neurotransmission, based on the joint versus independent actions of NO relative to NMDA receptors at pre- versus postsynaptic sites.

Keywords: Nitric oxide; Visual cortex; Glutamate receptor; NMDA receptor; Retrograde messenger; Axo-axonic interaction; LTP; Excitotoxicity; Immuno-electron microscopy

1. Introduction

Nitric oxide (NO), first identified as an endothelial vasodilator and a mediator of bactericidal and tumoricidal actions of macrophages, also is a putative neurotransmitter in the central and peripheral nervous systems (rev. in [8,14,23]). The first evidence that NO functions as a neurotransmitter was the observation that potent and selective inhibitors of the synthetic enzyme, i.e. neuronal nitric oxide synthase (nNOS), block NMDA receptor's stimulation of cGMP formation [8,24]. Since then, the majority of NO's action in the nervous system has been linked to NMDA receptor activation. For example, selective inhibitors of NOS or NO block NMDA receptor-mediated neurotransmitter release, glutamate neurotoxicity, and certain forms of long-term potentiation (LTP) in the hippocampal formation and cerebral cortex [15,17,23,42,55,62]. NO has also been shown to directly modulate NMDA receptor [40,42,46]. The critical link between NMDA receptors and NO generation appears to be Ca^{2+}, which permeates through opened NMDA channels, leading to the formation of a Ca^{2+}/calmodulin complex that can activate intracellularly localized nNOS (rev. in [23]). These results predict that nNOS occurs within neuronal profiles that are postsynaptic at synapses utilizing NMDA-type glutamate receptors. In accordance with this prediction, results of previous in situ hybridization studies indicate that nNOS cells in the forebrain contain high levels of NMDA receptor-mRNA [61]. However, the diffusion coefficient of Ca^{2+} within cells is very small (10^{-7} cm^2/s). Moreover, Ca^{2+} diffusion can be bounded further by local constrictions in processes, such as at spine necks [22,52] and at preterminal axons [43,44], or by the compet-

* Corresponding author. Center for Neural Science, 6 Washington Place, Rm 809, New York, NY 10003, USA. Fax: +1 (212) 995-4011; E-mail: chiye@cns.nyu.edu

PII S0006-8993(96)01147-X

itive cellular demands for free Ca^{2+}. Thus, the expression of nNOS and NMDA receptors within single cells does not ensure that the two molecules occur in sufficient proximity for immediate interaction. Even in the absence of NMDA receptors, nNOS can be activated by other neurotransmitters and biochemical cascades that elevate intracellular Ca^{2+} (rev. in [23]). These include the voltage-dependent Ca^{2+}-channels along the plasma membrane and the IP_3 and ryanodine receptors residing intracellularly [6,19,30,63]. Furthermore, LTP of the type depending on both NO and NMDA receptors persists in nNOS-knockout mice, indicating that other NOS isozymes (such as endothelial NOS) can compensate for the absence of nNOS [56]. These observations leave open the possibility that NMDA-receptors and nNOS may not always co-localize.

Thus, in this study, we employed dual immuno-electron microscopic methods to ascertain the spatial relationship of nNOS to NMDA receptors and to synapses. Specifically, we determined the following: whether nNOS occurs in the proximity of synapses, where regulation of transmitter release and receptor sensitivity occurs; whether nNOS occurs within spines receptive to glutamate through the NMDA receptor; whether nNOS occurs in the absence of NMDA receptors; whether the localization of nNOS and NMDA receptors is strictly postsynaptic or might also be presynaptic, allowing for NO generation following axo-axonic interactions.

2. Materials and methods

2.1. Preparation of tissue

Six adult male Sprague–Dawley rats (300–400 g b.wt, Hilltop) were deeply anesthetized by administering 50 mg/kg b.wt of Nembutal. During the initial phase of anesthesia, the rats were given an i.p. injection of 1 g/kg sodium diethyl dithiocarbamate, a zinc chelator, to decrease background immunogold staining caused by silver-intensification of endogenous zinc at glutamatergic synapses [66]. After confirming the complete absence of corneal reflex following light touch of the cornea and a minimum of 15 min following injection of sodium diethyl dithiocarbamate, transcardial perfusion was performed to obtain rat brains fixed with a mixture of aldehydes consisting of 3% acrolein and 4% paraformaldehyde, using previously detailed protocols [5]. Sections obtained from these brains were treated with 1% sodium borohydride dissolved in 0.1 M phosphate buffer (PB) to prevent continued fixation of tissue. These sections were used immediately afterwards for immunocytochemistry or stored for up to 7 days in phosphate-buffered saline consisting of 0.01 M PB combined with 0.9% NaCl and adjusted to pH 7.6 (PBS). Sodium azide in the concentration of 0.05% was added to PBS to minimize bacterial growth during storage.

2.2. Immunocytochemistry

The light and electron microscopic procedures for dual immunocytochemistry were as described previously with slight modifications [13]. In the first set of experiments, NMDA-R1 was visualized by the double-bridge PAP method [57] using a 1:200 dilution of rabbit anti-NMDA-R1 antiserum, characterized for its specificity in a previous study [5]. Here and in all other incubations with immunoreagents, PBS containing 1% BSA was used as diluent. Following a 2–3 day incubation at 6°C in this primary antiserum solution, the sections were rinsed in PBS, then incubated in a 1:50 dilution of goat anti-rabbit IgG (Jackson ImmunoResearch, West Grove, PA) for 1 h, followed by incubation in a 1:500 dilution of rabbit PAP (Jackson ImmunoResearch) for 1 h. Sections were then returned to the anti-rabbit IgG incubation buffer for 30 min, followed by a 30 min incubation in rabbit PAP. The peroxidase reaction product was generated by reacting the tissue with 0.022% of 3,3′-diaminobenzidine tetrahydrochloride (Aldrich Chem.) and 0.003% of hydrogen peroxide (Sigma Chem., St. Louis, MO) for 8–12 min.

The same sections were treated for the immunogold visualization of nNOS using a 1:500 dilution of guinea pig anti-nNOS antiserum. Specificity of this antiserum has been described in a previous publication [36]. Following 2–3 days of incubation in this antiserum at 6°C, the NOS-immunoreactive sites were visualized by incubating sections in a 1:100 dilution of biotinylated goat anti-guinea pig IgG (Vector Labs., Burlingame, CA) for 30 min, followed by a 30-min incubation in blocking buffer consisting of PBS, 1% BSA and 3% normal goat serum. This step was followed by a 3-h incubation in a 1:50 dilution of 1.4-nm gold conjugated goat anti-biotin (Goldmark, Phillipsburg, NJ) or 1-nm gold-conjugated streptavidin (Amersham, Arlington, IL) using PBS/BSA combined with 1% goat serum as diluent. Unlike the procedure of Chan et al. [13], gelatin was omitted from this incubation buffer and the blocking buffer. After postfixing with 0.25% glutaraldehyde buffered with PBS for 20 min, the sections were rinsed in citrate buffer (0.1 M, adjusted to pH 6.5–7.4 by titrating monohydrate and dihydrate trisodium salts [27]). Colloidal gold particles were visualized by reacting sections with a Silver IntensEM kit solution (Amersham) for 8–12 min at room temperature.

Three sets of control sections were generated alongside with the above. One set was incubated with the rabbit anti-NMDA-R1 antiserum, then treated according to the guinea pig immunogold procedure as described above for nNOS to determine whether the anti-guinea pig IgG recognizes the rabbit antiserum, i.e. the anti-NMDA-R1. A second set of sections was incubated with guinea pig anti-nNOS, then processed for the development of rabbit PAP, exactly as described above for the NMDA-R1 antiserum, to determine whether the anti-rabbit IgG recognizes the guinea pig antiserum, i.e. the anti-nNOS. A third set

was generated to determine whether the colloidal gold-conjugated reagents (streptavidin-gold and anti-biotin-gold) attach non-specifically to the peroxidase reaction product or whether the silver IntensEM kit solution generates background silver particles over the peroxidase reaction products. All reagents for the control set were the same as those used for the experimental.

In a second series of experiments, the immunolabels for NMDA-R1 and nNOS were switched. Sections were incubated for 2–3 days at 6°C in guinea pig anti-nNOS, then processed for the avidin-biotin-peroxidase complex formation [35] using the ABC Elite kit (Vector Labs.). The same sections were immunolabeled for NMDA receptors by the rabbit immunogold procedure using 1:200 dilution of rabbit anti-NMDA-R1, followed by a 3-h incubation in a 1:50 dilution of 1-nm colloidal gold conjugated goat anti-rabbit IgG (Amersham). The silver intensification was as described above. Two control sets of sections were processed alongside with these using the exact same reagents but in inappropriate combinations of secondary antibodies with respect to the primary antibodies. Thus, one set was incubated with rabbit anti-NMDA-R1 antiserum, then processed according to the guinea pig ABC-peroxidase procedure and the other set was incubated with the guinea pig anti-nNOS, followed by the procedure for rabbit immunogold labeling. Again, all reagents for the controls were exactly as used for the experimental.

2.3. Light and electron microscopic visualizations

A third of the immunolabeled sections were mounted on gelatin-coated slides, coverslipped and viewed using Zeiss's Axiophot or Olympus' BX-50-PM20 at magnifications ranging from 2.5× to 100× and photographed under DIC-Nomarski optics. The remaining sections were processed for electron microscopy. These were postfixed with 2% osmium tetroxide for 1 h, dehydrated with increasing concentrations of ethanol, and stained en bloc with 2% uranyl acetate/70% ethanol. The Vibratome-sections then were flat-embedded by sandwiching between two sheets of Aclar plastic using EMBED 812 (EMSciences, Port Washington, PA) as the embedding medium. Area 17 (visual cortex, Ocb 1) within the flat-embedded sections were identified under a light microscope using the atlas of Paxinos and Watson [58] for guidance. Specifically, sections were sampled from anterior-posterior levels where the splenium corpus callosum was absent, indicating that these were caudal to bregma by more than 5.3 mm. Within these sections, sampling was made more than 2 mm but less than 5 mm lateral from the midline. Portions of the coronal sections containing area 17 were re-embedded in capsules and mesas (trapezoids) spanning all layers of the visual cortex were prepared for ultrathin sectioning. Some of the ultrathin sections were further counterstained with lead citrate after ultrathin sectioning to optimize visualization of the fine structure, while others were examined without the lead citrate counterstain to optimize identification of electron density resulting from accumulation of the immunoperoxidase reaction product, particularly at postsynaptic densities. The ultrathin sections were examined using a JEOL 1200XL at magnifications ranging from 7500× up to 30 000×.

2.4. Identification of the fine structure

Sampling of tissue was restricted to surface-most portions of the immunolabeled Vibratome sections, where penetration by immunoreagents was expected to be maximal. Profiles seen under the electron microscope were categorized according to Peters et al. [59] as belonging to dendritic shafts, dendritic spines, preterminal axons, nonterminal axons, glial processes, perikarya of oligodendrocytes, astrocytes, endothelial cells or neurons. The remaining profiles were deemed unidentifiable. Immunoperoxidase reaction product was identified by the enhanced electron density that appeared flocculent. The silver-intensified colloidal gold (SIG) particles were identified by the clustering of maximally electron dense particles of irregular shapes, ranging in size from 50 to 300 nm in diameter and sometimes associated with a hole in the center of the cluster, caused by incomplete infiltration by the embedding medium. In order to avoid false-positive identification of immunogold labeling, the profiles were considered specifically labeled only if they contained three or more SIG particles and if these clusters recurred in adjacent ultrathin sections. In order to minimize false-negativities of immunoperoxidase labeling, electron microscopic analysis included ultrathin sections in which the lead citrate counterstain was omitted to enhance differentiation between electron dense organelles and those associated with deposits of peroxidase reaction products.

3. Results

3.1. Specificity of nNOS and NMDA-R1 immunocytochemistry as revealed by light microscopy

The distribution of nNOS was determined using a guinea pig polyclonal antiserum directed against a C-terminal peptide of nNOS [36]. The previous study using this antiserum demonstrated its specificity by showing that immunoreactivity was absent when applied to tissue from nNOS knock-out mice [36]. The anti-nNOS antiserum immunoprecipitates greater than 90% of NOS activity from brain homogenates, indicating that it recognizes enzymatically active form(s) of NOS (J.A. Mong and T.M. Dawson, unpubl. obs.) As expected [9,16,34], approximately 2% of cortical perikarya were intensely immunoreactive for nNOS. All of the immunoreactive perikarya were large and multipolar or bipolar: none were pyramidal (Fig. 1A,B).

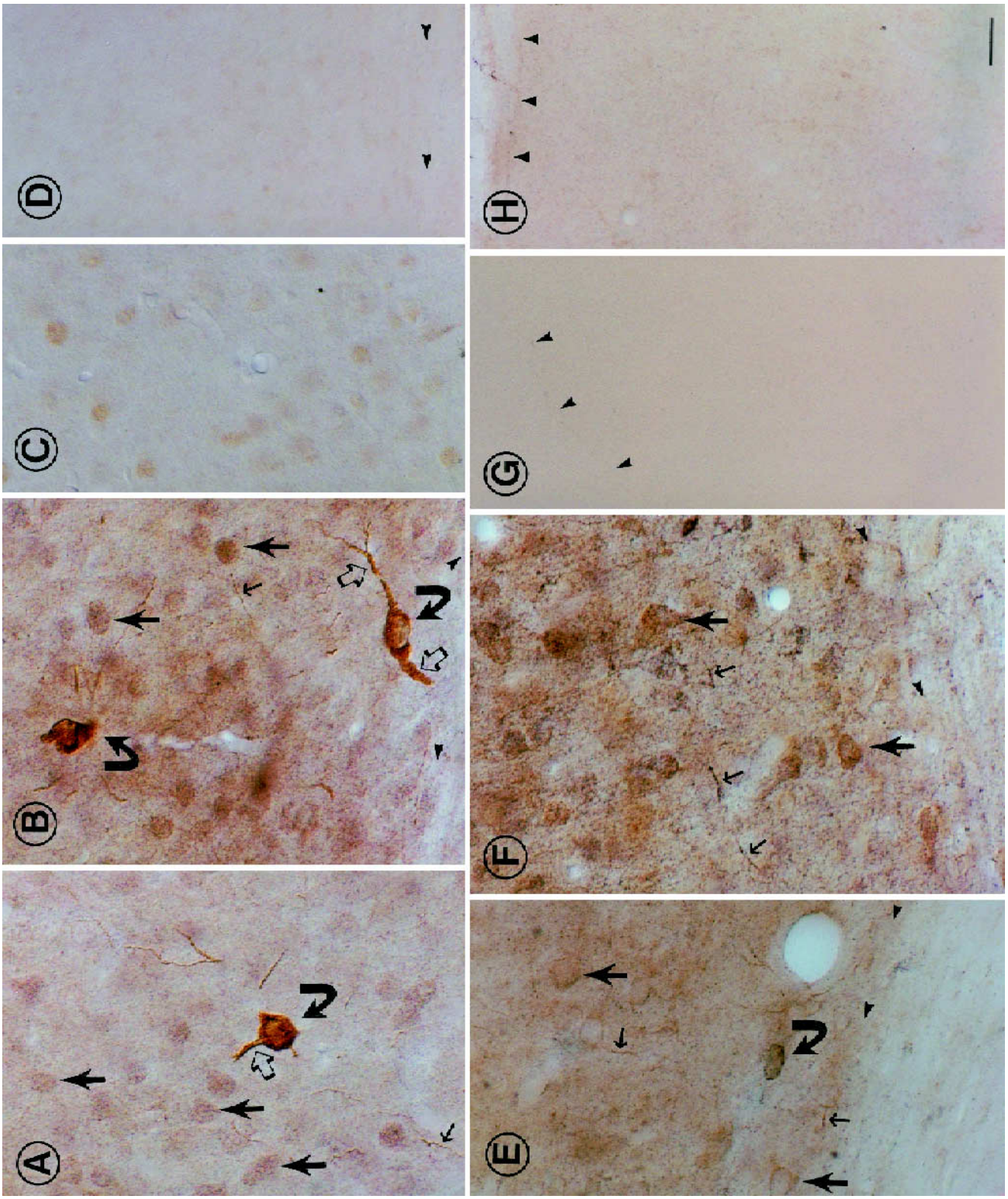
A
B
C
D
E
F
G
H

NMDA receptors were localized with a rabbit antibody directed against a C-terminal peptide of the NMDA-R1 subunit [5]. Results from previous studies characterizing the splice variants expressed in different brain regions indicate that this antibody would recognize the majority of NMDA-R1 subunits in the cerebral cortex. Although the antibody would not recognize splice variants lacking the C2 cassette, i.e. the splice variants, $NR1_{xx0}$, these are rare in the cerebral cortex [33,50,51,54,72]. Previous immunocytochemical studies also showed that spurious staining by the R1-subunit antiserum is minimal, since preadsorption of the NMDA-receptor antiserum abolishes immunolabeling [5]. When the anti-NMDA-R1 antiserum was recognized with a species-appropriate secondary antibody, there was detectable immunolabeling of neuronal perikarya (Fig. 1A,B). In addition, numerous immunolabeled processes were evident throughout the layers of the visual cortex (e.g. Fig. 1E for the infragranular layers). This pattern was identical to that described previously [5].

Although perikarya immunoreactive for both nNOS and NMDA-R1 were discernible by the silver-intensified gold (SIG) as well as the peroxidase labels, dually labeled perikarya were not detectable. This was probably due to the strong nNOS immunoreactivity that obscured the lower amounts of NMDA-R1 immunoreactivity within perikarya (Fig. 1A,B,E,F).

Before initiating dual electron microscopic labeling experiments with the nNOS and NMDA-R1 antisera, we evaluated the suitability and specificity of these antisera for double immunolabeling. The dual immunocytochemical procedure employed here requires visualization of one antigen by the immunoperoxidase method and of the other by the immunogold method using two primary antibodies made in different species [13]. Success of the dual labeling procedure requires that there be no cross-reactivity between the two secondary antibodies. The control experiments indicated that the antisera employed in this study fulfill the requisite criteria. Throughout the coronal sections, only pale and diffuse immunostaining was observed after applying the rabbit anti-NMDA-R1 antiserum to tissue, followed by anti-guinea pig IgG, whether using the peroxidase reaction product (Fig. 1D) or the SIG (Fig. 1H) as the label for light microscopic visualizations. When using SIG as label, incubation of sections in anti-guinea pig nNOS antiserum followed by the anti-rabbit IgG caused only light brown background labeling and no appearance of black labels (Fig. 1C). With using the peroxidase reaction product as labels, the nNOS control sections showed no labeling of any sort (Fig. 1G).

3.2. Subcellular distribution of nNOS immunoreactivity

nNOS immunoreactivity was detectable within dendritic shafts (Fig. 2), dendritic spines (Fig. 3) and axons (Fig. 4). Semi-quantitative analysis indicated that spinous labeling accounted for about a third of all immunoreactive profiles (63 of 138 immunoreactive profiles encountered) and is twice more frequent than dendritic shaft labeling (38 of the 138 profiles). Nearly all of the spinous labeling clustered over postsynaptic densities (59 of the 63 immunoreactive spines), and labeling over postsynaptic densities within dendritic shafts dropped to about half (21 of the 38 dendritic profiles). Along the dendritic plasma membrane, portions slightly removed from synapses also were immunoreactive (Figs. 2 and 3).

The frequency of nNOS-immunoreactive axon terminals was less than that for dendrites (21/138 or 15% of all immunoreactive profiles), and very few of these formed asymmetric synaptic junctions (Fig. 5). More frequently, immunoreactive terminals formed synaptic junctions with postsynaptic densities that were very thin (Fig. 4D) or intermediate in thickness (Fig. 4B,C). Apart from the abundance of synaptic vesicles, some nNOS-immunoreactive axons showed little in terms of synaptic specialization within the few planes of section sampled (Fig. 4A). Some of the nNOS-immunoreactive axons that formed symmetric junctions contained dense-cored vesicles (Fig. 4D), as would be predicted by the existence of nNOS in NADPH-diaphorase-containing neurons [9,16,34] which, in turn, contain the peptide, NPY [2,29,68].

The nNOS-immunoperoxidase reaction product rimmed small clear vesicles (Fig. 4A,D) and was associated with the cores of dense-cored vesicles as well (Fig. 4D). The association of nNOS immunoreactivity with vesicles,

Fig. 1. The distribution of immunoreactivity for nNOS in perikarya (curved arrows) and dendrites (open arrows) and for NMDA-R1 (large straight arrows) in perikarya of the rat visual cortex as revealed by light microscopic dual immunocytochemistry. The groups of arrowheads in panels B, D, E and F point to the white matter-grey matter boundary while the arrowhead groups in panels G and H point to pial surfaces. A,B: nNOS is immunolabeled by the guinea pig ABC-peroxidase procedure and appears orange-brown. The same section is immunolabeled for NMDA-R1 by the rabbit immunogold procedure yielding clusters of black particles. Panel A shows the supragranular layers, while panel B shows the deeper layers. The small arrows point to finer nNOS-immunoreactive processes that may be axonal. C and D show the degree of background labeling obtained in control sections. C shows a section incubated in guinea pig anti-nNOS, then processed by the rabbit immunogold procedure in the absence of rabbit anti-NMDA-R1. D shows a section incubated in rabbit anti-NMDA-R1, then processed by the guinea pig ABC-peroxidase procedure in the absence of guinea pig anti-nNOS. E,F: the immunolabels are switched from that shown in panels A and B. Hence, nNOS-immunoreactive perikarya are identifiable by the clusters of black particles while the NMDA-R1-immunoreactive perikarya appear light brown. Both light micrographs were obtained from the deep layers. The small arrows in panel E point to NMDA-R1-immunoreactive fine processes (orange-brown) while the small arrows in panel F point to nNOS-immunoreactive fine processes (black). The large hole to the right of the curved arrow in panel E is a cross-section of a blood vessel. Panels G and H show minimal labeling in control sections. Panel G shows a section incubated with guinea pig anti-nNOS, followed by incubations for the rabbit PAP procedure. Panel H shows a section incubated in rabbit anti-NMDA-R1, followed by incubations for the guinea pig immunogold procedure. Bar = 20 μm for all panels.

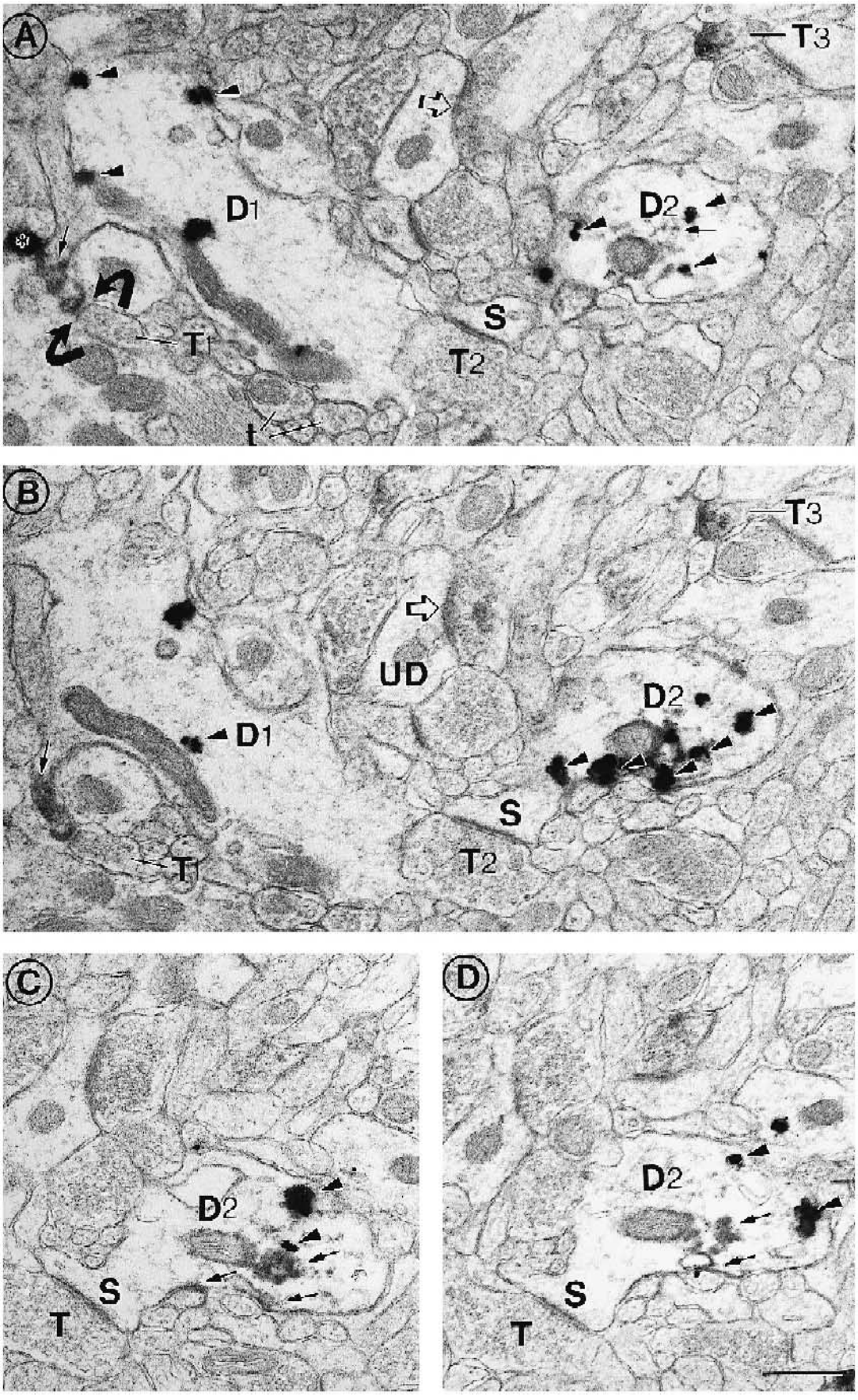
A
T3
D1
D2
S
T1
T2
t
B
T3
UD
D2
D1
S
T1
T2
C
D2
S
T
D
D2
S
T

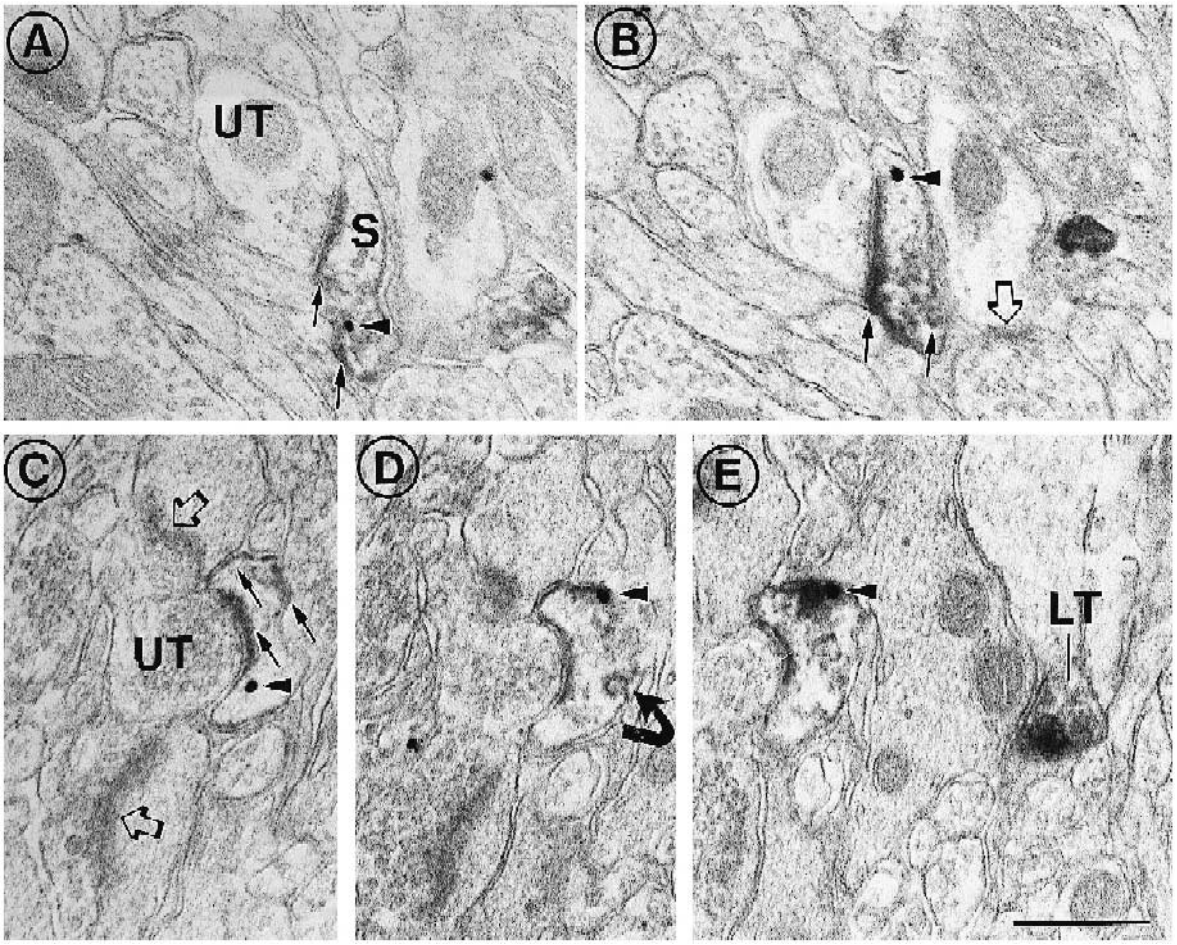

Fig. 3. Co-existence of NMDA-R1 with nNOS within dendritic spines as revealed by serially collected ultrathin sections from the supragranular layers of the rat visual cortex. Lead-citrate counterstain was omitted to facilitate detection of immunoperoxidase labels. In all panels, peroxidase label reflects nNOS-immunoreactivity (small arrows) and silver-intensified gold reflects NMDA-R1 immunoreactivity (arrowheads). Open arrows point to unlabeled postsynaptic densities. Panels A and B were taken from serially collected ultrathin sections. A small spine (S) receiving asymmetric synaptic input from an unlabeled terminal (UT) shows the presence of nNOS over a postsynaptic density (left small arrow) and extrajunctional plasma membranes (right small arrow). The same profile also shows recurrence of silver-intensified gold particles. Panels C–E, also are taken from serially collected ultrathin sections. An unlabeled terminal (UT in panel C) forms an asymmetric synaptic junction with a spine. The spine exhibits peroxidase reaction product along postsynaptic densities (lower left small arrow in C), extrajunctional plasma membrane (upper small arrow in C) and over an endocytotic vesicle (curved arrow in D). The same profile exhibits recurrence of silver-intensified gold particles. A labeled terminal (LT in panel E) also shows nNOS-immunoreactivity but no detectable NMDA-R1 immunoreactivity. Bar = 500 nm.

Fig. 2. A–D: co-existence of the NMDA-R1 subunit with nNOS in dendrites, as revealed by serially collected immunoelectron micrographs from the supragranular layer of the rat visual cortex. NMDA-R1 immunoreactivity is shown by the peroxidase labels (small arrows), and nNOS immunoreactivity by the SIG gold particles (arrowheads). Lead-citrate counterstain was omitted to facilitate detection of immunoperoxidase labels. Two medium-sized dendritic shafts (D1 and D2), exhibit both nNOS and NMDA-R1 immunoreactivity. In D1, NMDA-R1 occurs discretely within a spine protruding from the dendritic shaft along the left side. The spine head receives synaptic input from a terminal (T1). The two curved arrows in panel A point to the synaptic junction. The same dendritic shaft is in direct contact with two other terminals, ('t') which lack NMDA-R1 immunoreactivity postsynaptically. In D2, NMDA-R1 occurs at sites lacking synaptic associations within the four planes of section. Instead, NMDA-R1 immunoreactivity occurs along the plasma membrane (panel C) and surrounds a clear saccule (panels A and D). In panels B through D, it is apparent that a spine protrudes from D2. The spine receives synaptic input from a terminal (T2 in panels A and B) and forms an asymmetric synaptic junction without exhibiting detectable NMDA-R1 immunoreactivity. UD (panel B and recurring in all other panels) is an example of an unlabeled dendrite. The clear arrow in UD points to an unlabeled postsynaptic density. T3 (panels A and B) is a terminal showing NMDA-R1 immunoreactivity without nNOS-immunoreactivity. The asterisk to the left in panel A points to a non-recurrent SIG particle, reflecting non-specific labeling. Bar = 500 nm.

plasma membranes and postsynaptic densities is supportive of earlier findings of nNOS purifying from an insoluble fraction [31]. On the other hand, the distribution of nNOS immunoreactivity within the cytoplasm of axon terminals and dendrites supports initial findings that nNOS is enriched in the soluble fraction (rev. in [8]).

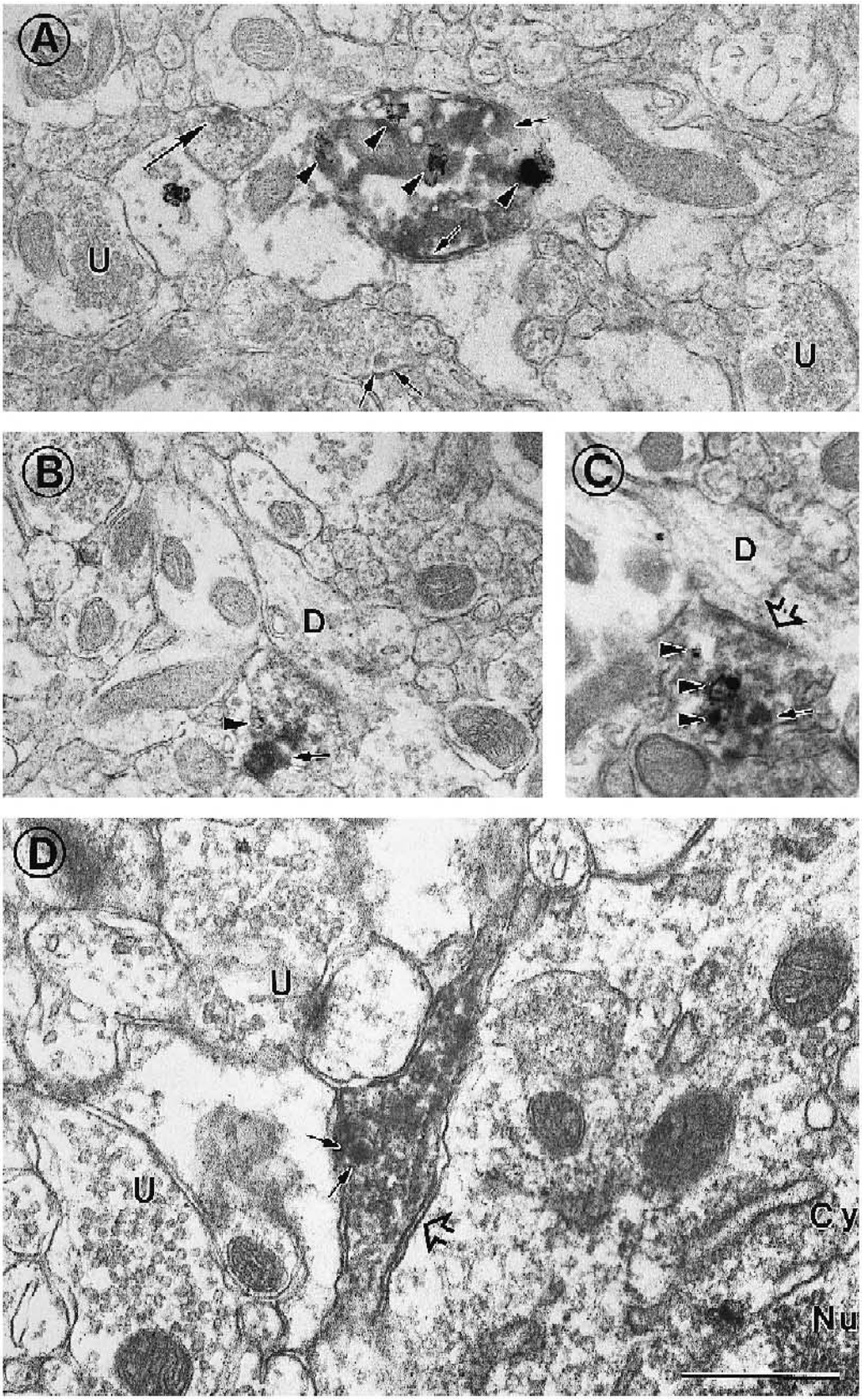

3.3. Subcellular distribution of NMDA-R1 immunoreactivity

Electron microscopy confirmed previous studies [5,20,37,60,64], namely that NMDA-R1 immunoreactivity is prevalent along the intracellular surface of dendritic plasma membranes (e.g. D2 of Fig. 2) and is most prominently clustered over postsynaptic densities within dendritic spines (e.g. spine of D1 in Fig. 2). When using the peroxidase reaction product as the label, immunoreactivity was evident as a flocculent electron dense material concentrating within spines and coating postsynaptic densities (Fig. 2). When using the SIG method, the label appeared much more electron-dense and discrete. Although the SIG particles tended to occur along the intracellular surface of plasma membranes, some resided slightly removed from the surface but still in the vicinity of postsynaptic densities (Fig. 3). Semi-quantitative analysis indicated that nearly half of all NMDA-R1-immunoreactive profiles were dendritic (75 of the 142 NMDA-R1-immunoreactive profiles encountered), with spines accounting for 23% and shafts accounting for 30% of them. All spines (32 of the 32 immunoreactive spines encountered) exhibited discrete immunolabeling over postsynaptic densities. Even though dendritic labeling was more frequent within shaft portions, only 60% of these (26 of the 43 immunoreactive dendritic shafts) were associated with postsynaptic densities within the planes of section. The immunoreactive sites within dendritic shafts included small clear saccules that are likely to be part of the smooth endoplasmic reticulum (D2 in Fig. 2D). This, and the observation that somatic immunolabeling is detectable by light microscopy, indicates that the antibody may recognize receptor molecules undergoing turnover. The extrajunctional labeling probably does not reflect the diffusion of immunolabels, since discretely labeled postsynaptic densities were observed immediately adjacent to unlabeled postsynaptic densities within the same profiles (not shown).

The accumulation of immunolabels along the intracellular surface of plasma membranes is in accordance with the most recent ideas about the receptor's membrane topology. Based on the hydropathicity profile of the receptor derived from its amino-acid sequence, the C-terminus has been predicted to reside intracellularly [33,50,51,72].

NMDA-R1 immunoreactivity at the postsynaptic density was more apparent with peroxidase labeling (Fig. 2A and B) than with SIG (Fig. 3). This may reflect stearic hindrance that affects penetration of immunogold reagents into organelles, such as postsynaptic densities. Thus, throughout this study, we interchanged the immunolabels for NMDA-R1 and nNOS to avoid bias in our assessment of the synaptic localization of the two molecules.

As noted in previous studies [5,64], NMDA-R1 immunoreactivity was present within axons as well. Immunoreactive axons accounted for nearly a third of all immunoreactive profiles (43 of the 142 NMDA-R1-immunoreactive profiles encountered). Most of the immunoreactive axons lacked morphologically identifiable synaptic targets (Fig. 4A). Where present, these axons formed synapses with thick (not shown), intermediate (Fig. 4B,C and Fig. 6) and thin (not shown) postsynaptic densities.

3.4. Co-existence of nNOS with NMDA-R1 in dendrites and axons

In order to optimize detection of both immunoperoxidase and SIG labels, sampling was done from regions of Vibratome sections that showed clear interface to the embedding matrix. Consequently, many of the dually labeled profiles exhibited robust immunolabeling but were missing portions of the plasma membrane or cytoplasmic matrices (e.g. Fig. 4C).

Dual labeling for nNOS and NMDA-R1 occurred predominantly at the shafts of dendrites (60% or 37 of the 62 dually labeled profiles identified by analysis of serially collected ultrathin sections) (Fig. 2) but was also detectable in spines (18% of the dually labeled profiles) (Fig. 3). Whether within spines or shafts of dendrites, most of the NMDA-R1 and nNOS immunolabels were in the vicinity of thick postsynaptic densities (Fig. 3) associated with synaptic junctions formed by unlabeled axon terminals.

Fig. 4. nNOS-immunoreactive terminals occur with and without NMDA-R1 immunoreactivity. In panels A–C, peroxidase label (small arrows) reflects NMDA-R1 immunoreactivity, while SIG particles (arrowheads) reflect nNOS immunoreactivity. In panel D, peroxidase label reflects nNOS immunoreactivity. A: a large terminal in the center of the panel exhibits immunoreactivity for both, nNOS and NMDA-R1. It contains numerous vesicles that are uniformly sized and shaped. NMDA-R1-immunoreactivity is evident along the plasma membrane (e.g. lower small arrow) and rimming vesicles. Four clusters of SIG particles occur within the cytoplasm and along the plasma membrane. A smaller terminal, to the left, exhibits a discrete patch of immunoreactivity for NMDA-R1 along the plasma membrane (long arrow) but no nNOS immunoreactivity. Synaptic targets of these terminals are not apparent within this plane of section. U's indicate unlabeled terminals for comparison with labeled terminals. A pair of arrows points to an unlabeled dense-cored vesicle, to be compared with the labeled dense-cored vesicle in panel D. Panels B and C were taken from serially collected ultrathin sections. In particular, the ultrathin section shown in panel C was taken exactly at the interface between tissue and the embedding medium. This is evident by the frequent interruptions of the plasma membrane but the numerous SIG particles. A terminal forms a junction with a postsynaptic density of intermediate thickness along the shaft of a dendrite (open arrow in profile, 'D'). This terminal exhibits heavy accumulation of peroxidase reaction product at a site away from the synapse. A total of four clusters of SIG particles occur in this profile. D: a terminal containing numerous small vesicles and one large dense-cored vesicle (two small arrows) is intensely nNOS-immunoreactive. SIG particles are not present. Double arrow in panel A points to an unlabeled dense-cored vesicle for comparison. A portion of its plasma membrane forms parallel alignment with perikaryal plasma membrane (large open arrow), indicating that this is a symmetric synaptic junction. Cy = perikaryal cytoplasm; Nu = nucleoplasm. Bar = 862 nm in A and B, 694 nm in C and 500 nm in D.

Occasionally, it was noted that NMDA-R1 immunoreactivity was contained within a spine receiving input from an unlabeled terminal while nNOS immunoreactivity was present only in the shaft portion of the same dendrite (D1 in Fig. 2).

Of the 62 dually labeled profiles, only 8, or 13%, were axonal. The dually labeled portions of terminals formed synaptic junctions along shafts of dendrites (Fig. 4B,C) or were without morphologically identifiable synaptic specialization within the planes of sampled sections (Fig. 4A). Asymmetric axo-spinous junctions formed by dually labeled terminals were not encountered.

3.5. Occurrence of NMDA-R1 and nNOS in separate neuronal profiles

Dual immunocytochemistry revealed that NMDA-R1-immunoreactive profiles lacking nNOS immunoreactivity

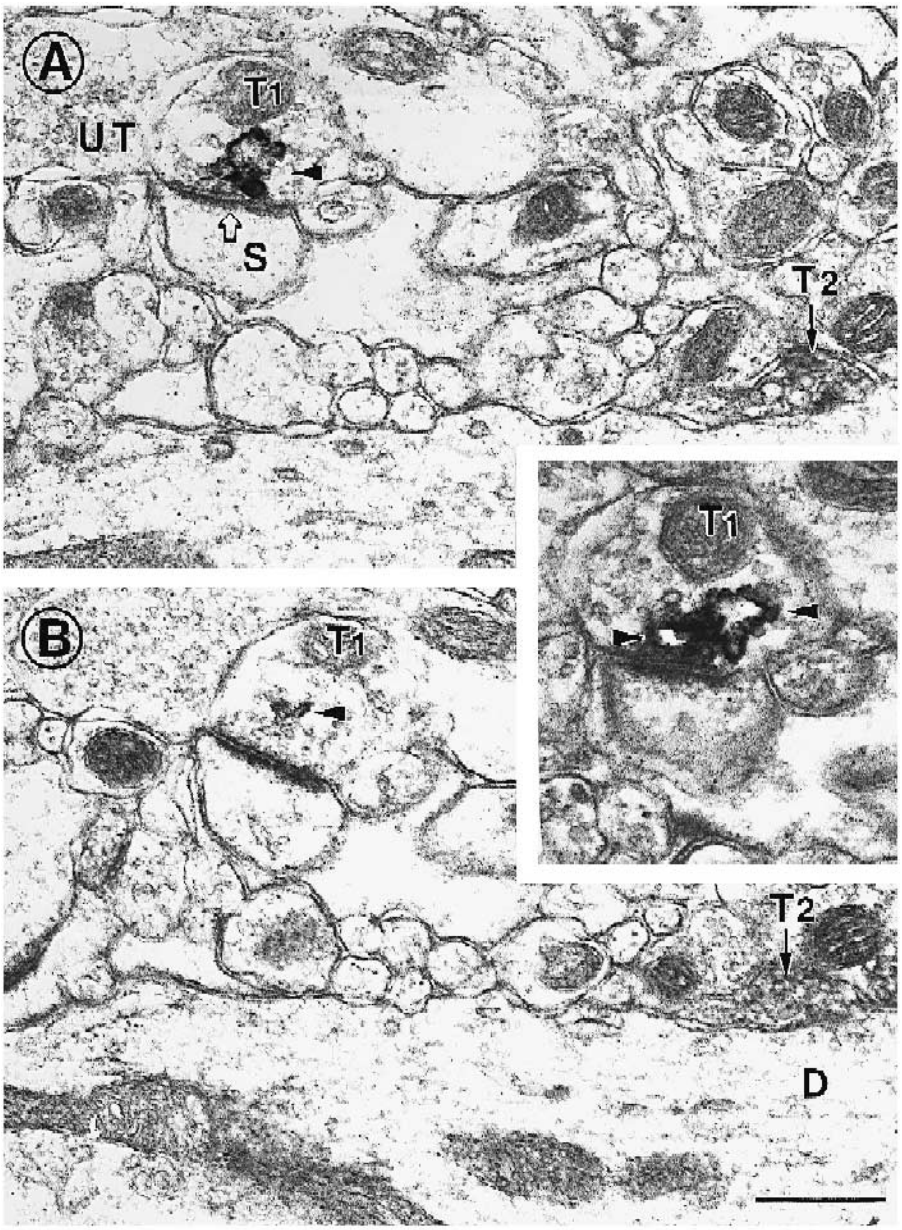

Fig. 5. A presynaptic terminal, immunoreactive for nNOS but NMDA-R1-negative, forms an asymmetric (presumably excitatory) axo-spinous junction. Peroxidase label reflects NMDA-R1 immunoreactivity (small arrows), while SG clusters reflect nNOS immunoreactivity (arrowheads). Panels A, B and inset in the middle are taken from serially collected ultrathin sections. Silver-intensified gold particles recur in T1. The synaptic target of T1 is a spine (S, open arrow points to the postsynaptic density). Another terminal, T2, is lightly immunoreactive for NMDA-R1. SIG particles are not detectable in T2. Here and in panel B, T2 courses next to a large dendritic shaft (D in panel B) but does not form an identifiable synaptic specialization within these planes of section. UT in panel A is one of many unlabeled terminals in their immediate vicinity, shown for comparison. Bar = 500 nm in panels A and B, 349 nm in inset.

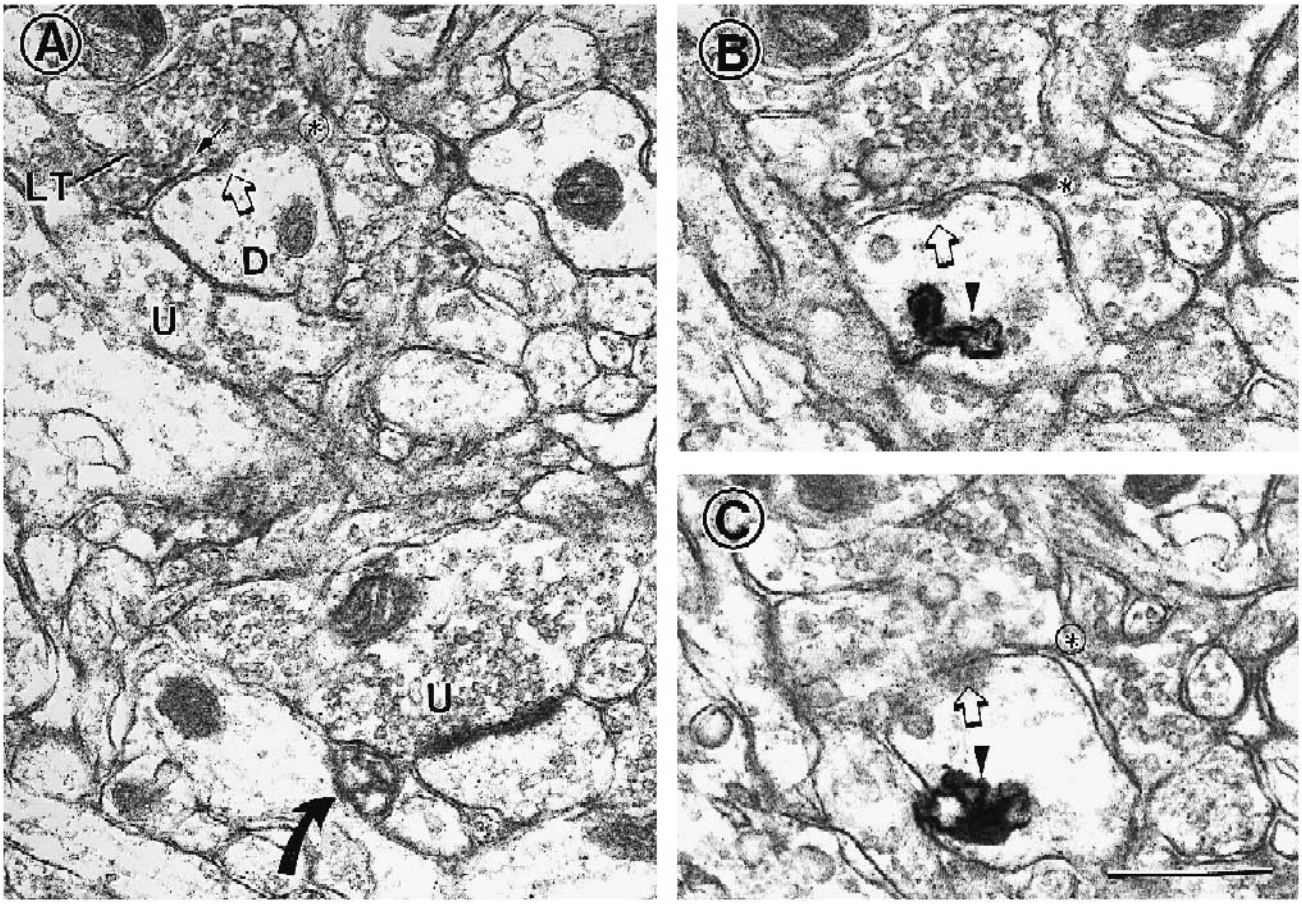

Fig. 6. Synaptic relationship between an NMDA-R1-immunoreactive terminal and a NOS-immunoreactive dendrite. A–C: open arrow points to the postsynaptic specialization. Peroxidase label reflects NMDA-R1 immunoreactivity (small arrow), while the SG particles reflect nNOS immunoreactivity (arrowheads). Serially collected sections are shown to demonstrate the recurrence of the SIG particles in a dendrite ('D' in panel A). Near threshold-level of immunoperoxidase reaction product is evident in the terminal, LT (panel A). Only those vesicles clustered towards the left of the circled asterisk are immunoreactive. U indicates one of many unlabeled terminals in the vicinity for comparison with the lightly labeled LT. Curved arrow in panel A: another NMDA-R1-immunoreactive axonal process. Bar = 700 nm in panel A and 500 nm in panels B and C.

also are present (e.g. T3 in Fig. 2). Conversely, not all of the nNOS-immunoreactive profiles were immunoreactive for NMDA-R1 (terminal, T1, in Fig. 5 and dendrite, D, in Fig. 6). In general, we took the presence of both SIG and immunoperoxidase labels in the immediate vicinity as indicators that both immunolabeling procedures had been successful. The presence of singly labeled profiles amongst dually labeled profiles also served as a confirmation that the currently employed immunocytochemical procedure was free of cross-reactivity, since all, or many more, of the profiles would otherwise have been dually labeled.

3.6. Electron microscopic results of control experiments

None of the neuronal or astrocytic profiles were immunolabeled under the control conditions testing for possible cross-reactivities of the secondary antibodies. Control experiments testing for non-specific association of SIG particles onto peroxidase reaction products also revealed no dually labeled profiles (not shown). The effect of silver-intensification of DAB reaction products was examined by applying the standard silver-intensification procedure to sections devoid of immunogold labeling. When the silver-intensification period was kept to the duration usually used for the dual labeling procedure, no silver particle was apparent over DAB reaction products (e.g. the DAB-labeled spine on D1 and the terminal, T3, in Fig. 2; LT in Fig. 3; Fig. 4D). When the silver-intensification period was lengthened by several minutes, a few silver particles began to accumulate over DAB reaction products (not shown). These, however, were much smaller than those that surround colloidal gold particles, and thus, could be distinguished easily from SIG labels.

4. Discussion

Results obtained from the present study provided answers to the four questions posed at the onset of the study (see Section 1). nNOS is not merely proximal to synapses

– it is most frequently at synapses and particularly within spines, where they are clustered directly over postsynaptic densities. NMDA-R1 is present at postsynaptic sites exhibiting nNOS immunoreactivity but this presence is not obligatory. Conversely, NMDA-R1 immunoreactivity occurs at synapses lacking nNOS immunoreactivity. Finally, nNOS occurs pre- as well as postsynaptically. The significance of these findings, in light of the methodological limitations posed by the dual immuno-electron microscopic technique, is discussed below.

4.1. Methodological considerations

4.1.1. Dually labeled profiles

Results from Western blots and preadsorption controls for both primary antisera and the discrete labeling within spine heads, terminals and dendritic shafts indicate that our immunocytochemical procedure reflects specific labeling of the fine neuronal processes. However, one of the limitations inherent in immunocytochemistry is that biological activity cannot be assumed at all labeled sites, since these may result from cross-reactions due to homologies of the antigen with unrelated proteins, the presence of non-functional peptide fragments resulting from turnover of the antigen, or diffusion of antigens and immunolabels. Furthermore, even if nNOS immunoreactivity were to reflect functional nNOS, NO still may not be generated at these sites without sufficient amounts of calmodulin and free intracellular Ca^{2+}. Previous immunocytochemical and biochemical results indicate that calmodulin is likely to be present in sufficient quantity to interact with nNOS at pre- and postsynaptic sites [18,25]. The present results, i.e. the co-existence of immunolabeling for nNOS and the NMDA-R1 (corresponding to $\zeta 1$ in mouse), a Ca^{2+}-permeable, ligand-gated channel subunit required for functional NMDA receptors [50], within dendritic shafts, spines and terminals provides further evidence that these nNOS-immunoreactive sites are where NO can be generated during excitatory synaptic activity.

Although NMDA-R1 immunoreactivity occurs mostly at postsynaptic sites, extrajunctional and intracellular sites also exhibit immunoreactivity. An obvious explanation for the extrajunctional plasmalemmal immunoreactivity is that the molecules are undergoing turnover. However, there is no reason to doubt that NMDA-R1 can be activated by L-glutamate overflow beyond synaptic clefts. Binding sites measured within frozen sections by receptor autoradiography may include intracellular sites that do not interact with synaptically released extracellular L-glutamate, but again, the possibility also exists that these NMDA-R1 subserve some function other than for synaptic transmission. One idea put forth by hippocampal physiologists is that some glutamate receptors occur as spares to be recruited following specific patterns of synaptic activity [41,45]. Perhaps some of the spares are stored intracellularly. Alternatively or in addition, even though these receptors cannot elicit membrane depolarization, they may yield a biologically significant signal that has yet to be appreciated following interaction with intracellular (including extravesicular) pools of L-glutamate.

The present dual immunocytochemical procedure is not amenable to quantitative assessment of the frequency of nNOS/NMDA-R1 co-existence. This is due to the fact that the immunodetection reflects underestimation caused by incomplete penetration of the immunoreagents and by the fixation of antigens that render them no longer recognizable by antisera. This problem is particularly severe for the detection of NMDA-R1 subunits by the silver-intensified gold method: we noted a drop in numerical density of NMDA-R1-immunoreactive profiles by greater than 5-fold when compared to the corresponding value obtained by the immunoperoxidase method and particularly over postsynaptic densities. Thus, the value of 1% for dually labeled dendrites and spines, among all dendritic profiles encountered during the survey, is reflective of the minimal degree of co-existence, even for tissue reacted by the immunoperoxidase procedure for detecting NMDA-R1 sites and the immunogold procedure for nNOS sites (the more favorable of the two labeling procedures).

4.1.2. Singly immunoreactive profiles

Although the singly immunoreactive profiles may reflect sites where NMDA receptors and nNOS operate independently, careful consideration must be made about potential false-negativities. Since immunoperoxidase labels are much more easily detected than are the pre-embedded silver-intensified immunogold labels, one can be fairly confident that the profiles exhibiting immunogold labels without the immunoperoxidase labels are, indeed, immunoreactive for only one antigen, particularly in cases where profiles in the immediate vicinity exhibit immunoperoxidase labels. Failure to detect immunoreactivity by the peroxidase label, particularly over electron dense organelles such as the postsynaptic density, was minimized further by omitting the lead citrate counterstain. Under this most stringent condition, we were still able to detect terminals and spines immunoreactive singly for nNOS or for the R1 subunit of NMDA receptors. This observation supports the idea that nNOS activation may sometimes occur independently of NMDA receptor activation and that NO generation is not obligatory following every NMDA-receptor activation.

4.1.3. Asymmetric junctions lacking NMDA-R1 immunoreactivity

It has long been established that asymmetric junctions exhibiting thick postsynaptic densities reflect excitatory synapses [26]. Yet, not all asymmetric junctions exhibited detectable levels of NMDA-R1 immunoreactivity. These sites probably reflect failures of immunodetection due to inadequate penetration of immunoreagents into tissue,

decrement of NMDA-R1 antigenicity due to the strong fixation, or stearic hindrance posed by other molecules or non-antigenic portions of the NMDA-R1 molecule. The possibility that some excitatory synapses operate by AMPA receptor activation alone also cannot be ruled out.

4.2. Significance of the synaptic localization of NMDA-R1 with NOS within dendrites

Dual immunocytochemistry revealed that nNOS and NMDA receptors occur together within dendrites and at sites receiving asymmetric (presumably excitatory [3,26]) synaptic inputs. These images suggest that nNOS activation can be evoked rapidly following NMDA receptor activation, with the interval limited primarily by the time necessary for Ca^{2+} to diffuse intracellularly from NMDA-R1 sites to where calmodulin and nNOS reside. Recent biochemical studies indicate that the proximity of nNOS to NMDA receptors may be ensured by a complex of postsynaptic density proteins, PSD-95, which can bind to nNOS's PDZ-containing domain and to the receptor's tSXV-concensus sequence [10]. The proximity of nNOS to NMDA-R1 may be sufficient to ensure that NO rises in the synaptic cleft within a time interval overlapping with presynaptic terminal depolarization, a physiological state hypothesized to confer selective NO receptivity upon axons (rev. in [23]) (see Section 4.4.).

In some cases, NMDA receptors and nNOS co-exist within dendrites receiving symmetric synaptic junctions. Since thin postsynaptic densities are rarely associated with excitatory inputs and usually occur in association with inhibitory and modulatory inputs [1,2,65], the proximity of NMDA-R1 and nNOS to symmetric synapses suggests that an excitatory input upon these dendrites may lead to generation of NO which operates retrogradely to modulate the release from non-glutamatergic, convergent axons (but see Section 4.4.). However, such retrograde action of NO would only be possible if the terminal forming the synaptic junction possesses appropriate binding sites for NO to regulate release. Clarification of this issue will have to wait until molecules mediating binding sites for NO release are discovered.

4.3. Significance of nNOS immunolabeling in spines

Previous light microscopic studies indicated that nNOS (and NADPH-diaphorase reactivity) in the cerebral cortex is enriched in a population of interneurons characterized by having medium to large cell bodies, varicose but aspiny or sparsely spiny dendrites, utilizing GABA as the neurotransmitter and storing NPY [9,16,34,67,68]. The present localization of the two antigens in spines may reflect their occurrence in the sparsely spiny, nNOS + /GABA + /NADPH diaphorase + /NPY + neurons detected previously by light microscopy. On the other hand, our current and previous [4] electron microscopic studies indicate that approximately 30 to 75% of nNOS-labeled profiles are spinous, depending on the region sampled. Judging from this prevalence of spinous labeling, it is more likely that at least some of the labeled spines belong to spiny neurons, i.e. the stellate and pyramidal neurons, even if their perikarya and proximal dendrites contain levels of nNOS that are too low to be detectable by light microscopy. All but one of the light microscopic studies known to us [70] reported that nNOS is absent within spiny neurons. This may be due to the requirement that perikarya and dendrites be stained intensely for light microscopic detection. Study is currently underway to determine whether or not the nNOS-immunolabeled spines belong to spiny neurons, identified by intracellular filling with biocytin.

4.4. Significance of the occurrence of nNOS and NMDA receptors in axons

As expected, terminals immunoreactive for nNOS exhibit the characteristic morphological features of GABA/NPY inhibitory interneurons, i.e. the formation of symmetric synaptic junctions with dendritic shafts and perikarya [1,2,29,65]. Occasionally, nNOS-positive terminals form asymmetric axo-spinous junctions. This morphological characteristic is rarely, if ever, associated with GABAergic axon terminals. Thus, this observation also is indicative of the presence of nNOS in non-GABAergic, most likely glutamatergic [3,5,26], axon terminals. Such profiles are further indications that nNOS exists in excitatory, spiny neurons of the cerebral cortex, albeit at low levels.

The co-existence of NMDA-R1 with nNOS in axon terminals suggests that activation of NMDA-R1 here may be triggered by the release of glutamate from other near-by terminals, leading to the activation of presynaptic NMDA receptors, an influx of Ca^{2+} and a subsequent activation of nNOS, independent of action potentials propagating in those terminals. Conversely, the presence of axons immunolabeled for nNOS with and without NMDA receptors indicates that NO might be generated in axons independently of glutamatergic synaptic transmission, since the arrival of action potentials in the terminal would evoke Ca^{2+} influx via voltage-sensitive Ca^{2+}-channels [6]. This event could, in turn, activate nNOS. Yet another scenario for nNOS activation within axons is that Ca^{2+}-permeable AMPA-type glutamate receptors participate in raising axonal levels of Ca^{2+}. In support of this idea, recent work indicates that most of the nNOS cells in the forebrain lack detectable levels of GluR2 expression (which confers Ca^{2+}-impermeability upon AMPA receptors) [12] and that presynaptic AMPA receptors lack GluR2, regardless of their cells of origin [20].

The consequence of NO released from axon terminals may be to enhance transmitter release through a feedback loop or by modulating neighboring terminals. Neurochemical results were the first to indicate that NMDA receptors

occur presynaptically to enhance the release of dopamine, acetylcholine, norepinephrine or glutamate [11,21,32,38,39,48,49,69]. However, with the introduction of NO as a retrograde messenger, others had offered reinterpretation of the neurochemists' results, namely that NO generated following activation of postsynaptic NMDA receptors act retrogradely to enhance transmitter release [28]. The present observations of nNOS and NMDA receptors in presynaptic and postsynaptic processes suggest that both biochemical cascades are possible.

Besides the issue discussed above, we speculate that NMDA receptors on terminals may confer NO-binding to those recently activated terminals for enhancing neurotransmitter release. It has been noted that coincident elevation of presynaptic activity, NO generation and NMDA receptor activation can, in some cases, lead to long-lasting enhancement of neurotransmitter release which, in turn, underlies long-term potentiation (LTP) [23]. We hypothesize that NMDA receptors on axons would be the very ones activated during delivery of a tetanus suitable for LTP, since synaptically released glutamate would diffuse towards postsynaptic AND presynaptic membranes. Those terminals endowed with NMDA receptors AND participating in the tetanus would have activatable NMDA receptors, because depolarization that propagates down those axons will have relieved the Mg^{2+}-block upon NMDA receptors [47]. By requiring activation of presynaptic NMDA receptors for NO receptivity, those presynaptic sites remaining silent during NO generation would be excluded from undergoing the cellular changes leading to enhanced neurotransmitter release, because NMDA receptors on these terminals would be blocked by Mg^{2+} and/or not be occupied by the ligand. In our opinion, the best support for this hypothesis comes from Murphy's group that reports a conversion of LTP to synaptic depression by delivering NO during the LTP-induction period [53]. Interestingly, their paradigm involved pharmacological blockage of NMDA receptors, based on the reasoning that, when providing an exogenous source of NO, postsynaptic NMDA receptors ought to be bypassed in order to prevent the release of endogenous NO. However, we reason that synaptic depression is caused by APV-blockage of *pre*synaptic NMDA receptors, which renders those axons no longer receptive to NO at binding sites linked to the enhancement of neurotransmitter release. This idea is consistent with the observations of Zhuo et al. [71] and others showing NO-dependent LTP when NMDA receptors (pre or post) remain unblocked. Boulton et al. [7] also reported on NO-mediated synaptic depression. It is important to note that their application of NO preceded, rather than concur with, tetanus delivery. Our working hypothesis does not contradict Boulton or Murphy's results [7,53], for NO could cause decrease of transmitter release among inactive (or D(−)-AP5-blocked) axons while also enhancing transmitter release from activated axons. How exactly might the activation of presynaptic NMDA receptors confer NO-binding and how might NO-binding to molecules in the terminal enhance neurotransmitter release? These are questions for the future.

Acknowledgements

We thank C.G. Go, X.-Z. Song, B. Taylor, Z. Shusterman and Mian Hou for their excellent technical assistance. We thank J.A. Mong, M. Fotuhi, and A.H. Sharp for assistance in preparing the antibodies. We are grateful to Alev Erisir for her careful reading of the manuscript. The study was supported by N.I.H. Grants EY08055 and NS30944 (Shannon Award), the NSF Presidential Faculty Fellowship RCD 92-53750 and the Human Frontiers Science Program RG-16/93 to C.A. T.M.D. is supported by U.S.P.H.S. Grants NS33277 and NS01578 and grants from the American Health Assistance Foundation, International Life Sciences Institute and the Beeson's Scholar in Aging Research.

References

[1] Aoki, C. and Pickel, V.M., Neuropeptide Y in the cerebral cortex and the caudate-putamen nuclei: ultrastructural basis for interactions with GABAergic and non-GABAergic neurons, *J. Neurosci.*, 9 (1989) 4333–4354.

[2] Aoki, C. and Pickel, V.M., Neuropeptide Y in cortex and striatum, In *Central and Peripheral Significance of Neuropeptide Y and its Related Peptides*, *Ann. NY Acad. Sci*., 611 (1990) 186–205.

[3] Aoki, C. and Kabak, S., Cholinergic terminals in the cat visual cortex: Ultrastructural basis for interaction with glutamate-immunoreactive neurons and other cells, *Vis. Neurosci*., 8 (1992) 177–191.

[4] Aoki, C., Fenstemaker, S., Lubin, M. and Go, C.-G., Nitric oxide synthase in the visual cortex of monocular monkeys as revealed by light and electron microscopic immunocytochemistry, *Brain Res*., 620 (1993), 97–113.

[5] Aoki, C., Venkatesan, C., Go, C.-G., Mong, J.A. and Dawson, T.M., Cellular and subcellular localization of NMDA-R1 subunit immunoreactivity in the visual cortex of adult and neonatal rats, *J. Neurosci*., 14 (1994) 5202–5222.

[6] Augustine, G.J., Charlton, M.P. and Smith, S.J., Calcium action in synaptic transmitter release, *Annu. Rev. Neurosci*., 10 (1987) 633–693.

[7] Boulton, C.L., Irving, A.J., Southam, E., Potier, B., Garthwaite, J. and Collingridge, G.L., The nitric oxide-cyclic GMP pathway and synaptic depression in rat hippocampal slices, *Eur. J. Neurosci*., 6 (1994) 1528–1535.

[8] Bredt, D.S. and Snyder, S.H., Nitric oxide, a novel neuronal messenger, *Neuron*, 8 (1992) 3–11.

[9] Bredt, D.S., Glatt, C.E., Hwang, P.M., Fotuhi, M., Dawson, T.M. and Snyder S.H., Nitric oxide synthase protein and mRNA are discretely localized in neuronal populations of the mammalian CNS together with NADPH diaphorase, *Neuron*, 7 (1991) 615–624.

[10] Brenman J.E., Chao, D.S., Gee, S.H., McGee, A., Craven, S.E., Santillano, D.R., Huang, F., Xia, H., Peters, M.F., Froehner, S.C. and Bredt, D.S. Interaction of nitric oxide synthase with the postsynaptic density protein PSD-95 and alpha 1-syntrophin mediated by PDZ domains, *Cell*, 84 (1996) 757–767.

[11] Bustos, G., Abarca, J., Forray, M.I., Gysling, K., Bradberry, C.W. and Roth, R.H., Regulation of excitatory amino acid release by

N-methyl-D-aspartate receptors in rat striatum: in vivo microdialysis studies, *Brain Res*., 585 (1992) 105–115.
[12] Catania, M.V., Tölle, T.R. and Monyer, H., Differential expression of AMPA receptor subunits in NOS-positive neurons of cortex, striatum and hippocampus, *J. Neurosci*., 15 (1995) 7046–7061.
[13] Chan, J., Aoki, C. and Pickel, V.M., Optimization of differential immunogold-silver and peroxidase labeling with maintenance of ultrastructure in brain sections before plastic embedding, *J. Neurosci. Methods*, 33 (1990) 113–127.
[14] Dawson, T.M. and Snyder, S.H., Gases as biological messengers: nitric oxide and carbon monoxide in the brain, *J. Neurosci*., 14 (1994) 5147–5159.
[15] Dawson, T.M. and Dawson, V.L., Nitric oxide: actions and pathological roles, *Neuroscientist*, 1 (1995) 7–18.
[16] Dawson, T.M., Bredt, D.S., Fotuh, I.M., Hwang, P.M. and Snyder, S.H., Nitric oxide synthase and neuronal NADPH diaphorase are identical in brain and peripheral tissues, *Proc. Natl. Acad. Sci. USA*, 88 (1991) 7797–7801.
[17] Dawson, V.L., Dawson, T.M., Bartley, D.A., Uhl, G.R. and Snyder, S.H., Mechanisms of nitric oxide mediated neurotoxicity in primary brain cultures, *J. Neurosci*., 13 (1993), 2651–2661.
[18] DeLorenzo, R.J., Role of calmodulin in neurotransmitter release and synaptic function, *Ann. NY Acad. Sci*., 356 (1980) 92–109.
[19] Ellisman, M.H., Deerinck, T.J., Ouyang, Y., Beck, C.F., Tanksley, S.J., Walton, P.D., Airey, J.A. and Sutko, J.L., Identification and localization of ryanodine binding proteins in the avian central nervous system, *Neuron*, 5 (1990) 135–146.
[20] Farb, C.R., Aoki, C. and LeDoux, J.E., Differential localization of NMDA and AMPA receptors in the lateral and basal nuclei of the amygdala: a light and electron microscopic study, *J. Comp. Neurol*., 362 (1995) 86–108.
[21] Fink, K., Bonisch, H. and Gothert, M., Presynaptic NMDA receptors stimulate noradrenaline release in the cerebral cortex, *Eur. J. Pharmocol*., 185 (1990) 115–117.
[22] Gamble, E. and Koch, C., The dynamics of free calcium in dendritic spines in response to repetitive synaptic input, *Science*, 236 (1987) 1311–1315.
[23] Garthwaite, J. and Boulton C.L., Nitric oxide signaling in the central nervous system, *Annu. Rev. Physiol*., 57 (1995) 683–706.
[24] Garthwaite, J., Charles, S.L. and Chess-Williams, R., Endothelium-derived relaxing factor release on activation of NMDA receptors suggests role as intercellular messenger in the brain, *Nature*, 336 (1988) 385–388.
[25] Grab, D.J., Carlin, R.K. and Siekevitz, P., The presence and functions of calmodulin in the postsynaptic density, *Ann. NY Acad. Sci*., 356 (1980) 55–71.
[26] Gray, E.G., Axo-somatic and axo-dendritic synapses of the cerebral cortex, *J. Anat*., 93 (1959) 420–433.
[27] Hacker, G.W., Grimelius, L., Danscher, G., Bernatzky, G., Muss, W., Adam, H. and Thurner, J., Silver acetate autometallography: an alternative enhancement technique for immunogold-silver staining (IGSS) and silver amplification of gold, silver, mercury and zinc in tissues, *J. Histotechnol*., 11 (1988) 213.
[28] Hanbauer, I., Wink, D., Osawa, Y., Edelman, G.M. and Gally, J.A., Role of nitric oxide in NMDA-evoked release of [^{3}H]-dopamine from striatal slices, *NeuroReport*, 3 (1992) 409–412.
[29] Hendry, S.H.C., Jones, E.G. and Emson, P.C. Morphology, distribution and synaptic relations of somatostatin- and neuropeptide Y-immunoreactive neurons in rat and monkey neocortex, *J. Neurosci*., 4 (1984) 2497–2517.
[30] Henzi, V. and MacDermott, A.B., Characteristics and function of Ca^{2+}- and inositol 1,4,5-trisphosphate-releasable stores of Ca^{2+} in neurons, *Neuroscience*, 46 (1992), 251–273.
[31] Hiki, K., Hattori, R., Kawai, C. and Yui, Y., Purification of insoluble nitric oxide synthase from rat cerebellum, *J. Biochem*., 111 (1993) 556–558.
[32] Hirsch, D.B., Steiner, J.P., Dawson, T.M., Mammen, A., Hayek, E. and Snyder, S.H., Neurotransmitter release regulated by nitric oxide in PC-12 cells and brain synaptosomes, *Curr. Biol*., 3 (1993) 749–754.
[33] Hollman, M., Boulter, J., Maron, C., Beasley, L., Sullivan, J., Pecht, G. and Heinemann, S., Zinc potentiates agonist-induced currents at certain splice variants of the NMDA receptor, *Neuron*, 10 (1993) 943–954.
[34] Hope, B.T., Michael, G.J., Knigge, K.M. and Vincent, S.R., Neuronal NADPH diaphorase is a nitric oxide synthase, *Proc. Natl. Acad. Sci. USA*, 88 (1991) 2811–2814.
[35] Hsu, S., Raine, L. and Fanger, H., Use of avidin-biotin-peroxidase complex (ABC) in immunoperoxidase techniques: a comparison between ABC and unlabeled antibody (PAP) procedures, *J. Histochem. Cytochem*., 29 (1981) 577–580.
[36] Huang, P.L., Dawson, T.M., Bredt, D.S., Snyder, S.H. and Fishman, M.C., Targeted disruption of the neuronal nitric oxide synthase gene, *Cell*, 75 (1993) 1279–1288.
[37] Huntley, G.W., Vickers, J.C. and Morrison, J.H., Cellular and synaptic localization of NMDA and non-NMDA receptor subunits in neocortex: organizational features related to cortical circuitry, function and disease, *Trends Neurosci*., 17 (1994) 536–543.
[38] Krebs, M.O., Desce, J.M., Kemel, M.L., Gauchy, C., Godeheu, G., Cheramy, A. and Glowinski, J., Glutamatergic control of dopamine release in the rat striatum: evidence for presynaptic *N*-methyl-D-aspartate receptors on dopaminergic nerve terminals, *J. Neurochem*., 56 (1991) 81–85.
[39] Lehmann, J., Valentino, R. and Robine, V., Cortical norepinephrine release elicited in situ by *N*-methyl-D-aspartate (NMDA) receptor stimulation: a microdialysis study, *Brain Res*., 599 (1992) 171–174.
[40] Lei, S.Z., Pan, Z.-H., Aggarwal, S.K., Chen, H.-S.V., Hartman, J., Sucher, N.J. and Lipton, S.A., Effect of nitric oxide production on the redox modulatory site of the NMDA receptor-channel complex, *Cell*, 8 (1992) 1087–1099.
[41] Liao, D., Hessler, N.A. and Malinow, R., Activation of postsynaptically silent synapses during pairing-induced LTP in CA1 region of hippocampal slice, *Nature*, 375 (1995) 400–404.
[42] Lipton, S.A., Choi, Y.B., Pan, Z.H., Lei, S.Z., Chen, H.S., Sucher, N.J., Loscalzo, J., Singel, D.J. and Stamler, J.S., A redox-based mechanism for the neuroprotective and neurodestructive effects of nitric oxide and related nitroso-compounds, *Nature*, 364 (1993) 626–632.
[43] Llinás, R., Steinberg, I.Z. and Walton, K., Presynaptic calcium currents and their relation to synaptic transmission: voltage clamp study in squid giant synapse and theoretical model for the calcium gate, *Proc. Natl. Acad. Sci. USA*, 73 (1976) 2918–3922.
[44] Llinás, R., Sugimori, M. and Silver, R.B., Microdomains of high calcium concentration in a presynaptic terminal, *Science*, 256 (1992) 677–679.
[45] Lynch, G. and Baudry, M., The biochemistry of memory: a new and specific hypothesis, *Science*, 224 (1984) 1057–1063.
[46] Manzoni, O. and Bockaert, J., Nitric oxide synthase activity endogenously modulates NMDA receptors, *J. Neurochem*., 61 (1993) 368–370.
[47] Mayer, M.L. and Westbrook, G.L., The physiology of excitatory amino acids in the vertebrate central nervous system, *Prog. Neurobiol*., 28 (1987) 198–276.
[48] Moghaddam, B., Gruen, R.J., Roth, R.H., Bunney, B.S. and Adams, R.N., Effect of L-glutamate on the release of striatal dopamine: in vivo dialysis and electrochemical studies, *Brain Res*., 518 (1990) 55–60.
[49] Montague, P.R., Gancayco, C.D., Winn, M.J., Marchase, R.B. and Friedlander, M.J., Role of NO production in NMDA receptor mediated neurotransmitter release in cerebral cortex, *Science*, 263 (1994) 973–977.
[50] Monyer, H., Sprengel, R., Schoepfer, R., Herb, A., Higuchi, M.,

Lomeli, H., Burnashev, N., Sakmann, B. and Seeburg, P.H., Heteromeric NMDA receptors: molecular and functional distinction of subtypes, *Science*, 256 (1992) 1217–1221.
[51] Mori, H. and Mishina, M., Structure and function of the NMDA receptor channel, *Neuropharmacology*, 34 (1995) 1219–1237.
[52] Müller, W. and Connor, J.A., Dendritic spines as individual neuronal compartments for synaptic Ca^{2+} responses, *Nature*, 354 (1991) 73–79.
[53] Murphy, K.P.S.J., Williams, J.H., Bettache, N. and Bliss, T.V.P., Photolytic release of nitric oxide modulates NMDA receptor-mediated transmission but does not induce long-term potentiation at hippocampal synapses, *Neuropharmacology*, 33 (1994) 1375–1385.
[54] Nakanishi, N., Axel, R. and Schneider, N.A., Alternative splicing generates functionally distinct *N*-methyl-D-aspartate receptors, *Proc. Natl. Acad. Sci. USA*, 89 (1992) 8552–8556.
[55] Nowicky, A.V. and Bindman, L.J., The nitric oxide synthase inhibitor, *N*-monomethyl-L-arginine blocks induction of a long-term potentiation-like phenomenon in rat medial frontal cortical neurons in vitro, *J. Neurophysiol*., 70 (1993) 1255–1259.
[56] O'Dell, T.J., Huang, P.L., Dawson, T.M., Dinerman, J.L., Snyder, S.H., Kandel, E.R. and Fishman, M.C., Endothelial NOS and the blockade of LTP by NOS inhibitors in mice lacking neuronal NOS, *Science*, 265 (1994) 542–546.
[57] Ordronneau, P., Lindstrom, P.B.M. and Petrusz, P., Four unlabeled antibody bridge techniques: A comparison, *J. Histochem. Cytochem*., 29 (1981) 1397–1404.
[58] Paxinos, G. and Watson, C., *The Rat Brain in Stereotaxic Coordinates, 2nd edn.*, Academic Press, New York.
[59] Peters, A., Palay, S.L. and Webster, H.D., *The Fine Structure of the Nervous System, 3rd edn.*, Oxford, New York, 1991.
[60] Petralia, R.S., Yokotani, N. and Wenthold, R.J., Light and electron microscope distribution of the NMDA receptor subunit NMDAR1 in the rat nervous system using a selective anti-peptide antibody, *J. Neurosci*., 14 (1994) 667–696.
[61] Price, R.H., Mayer, B. and Beitz, A.J., Nitric oxide synthase neurons in rat brain express more NMDA receptor mRNA than non-NOS neurons, *NeuroReport*, 4 (1993) 807–810.
[62] Schuman, E.M. and Madison, D.V., Nitric oxide and synaptic function, *Annu. Rev. Neurosci*., 17 (1994) 153–183.
[63] Sharp, A.H., McPherson, P.S., Dawson, T.M., Aoki, C., Campbell, K.P. and Snyder, S.H., Differential immunohistochemical localization of inositol 1,4,5-triphosphate and ryanodine-sensitive Ca^{2+}-release channels in rat brain, *J. Neurosci*., 13 (1993) 3051–3063.
[64] Siegel, S.J., Brose, N., Janssen, W.G., Gasic, G.P., Jahn, R., Heinemann, S.F. and Morrison, J.H., Regional, cellular, and ultrastructural distribution of *N*-methyl-D-aspartate receptor subunit 1 in monkey hippocampus, *Proc. Natl. Acad. Sci. USA*, 91 (1994) 564–568.
[65] Somogyi, O. and Soltesz, I., Immunogold demonstration of GABA in synaptic terminals of intracellularly recorded, horseradish peroxidase-filled basket cells and clutch cells in the Cat's visual cortex, *Neuroscience*, 19 (1986) 1051–1065.
[66] Veznedaroglu, E. and Milner, T.A., Elimination of artifactual labeling of hippocampal mossy fibers seen following pre-embedding immunogold-silver technique by pretreatment with zinc chelator, *Microscopy Res. Tech.*, 23 (1992), 100–101.
[67] Vincent, S.R. and Kimura, H., Histochemical mapping of nitric oxide synthase in the rat brain, *Neuroscience*, 46 (1992) 755–784.
[68] Vincent, S.R., Johansson, O., Hokfelt, T., Skirboll, L., Elde, R.P., Terenius, L., Kimmel, J. and Goldstein, M., NADPH-diaphorase: a selective histochemical marker for striatal neurons containing both somatostatin- and avian pancreatic polypeptide (APP)-like immunoreactivities, *J. Comp. Neurol*., 217 (1983) 252–263.
[69] Wang, J.K.T., Andrews, H. and Thukral, V., Presynaptic glutamate receptors regulate noradrenaline release from isolated nerve terminals, *J. Neurochem*., 58 (1992), 204–211.
[70] Wendland, B., Schweizer, F.E., Ryan, T., Nakane, M., Murad, F., Scheller, R.H. and Tsien, R.W., Existence of nitric oxide synthase in rat hippocampal pyramidal cells, *Proc. Natl. Acad. Sci. USA*, 91 (1994) 2151–2155.
[71] Zhuo, M., Small, S.A., Kandel, E.R. and Hawkins, R.D., Nitric oxide and carbon monoxide produce activity-dependent long-term synaptic enhancement in hippocampus, *Science*, 260 (1993) 1946–1950.
[72] Zukin, R.S. and Bennett, M.V.L., Alternatively spliced isoforms of the NMDAR1 receptor subunit, *Trends Neurosci*., 18 (1995) 306–313.